Fermi National Accelerator Laboratory

FERMILAB-FN-594

MUSIM
Program to Simulate Production and Transport of Muons in Bulk Matter

A. Van Ginneken

Fermi National Accelerator Laboratory
P.O. Box 500, Batavia, Illinois 60510

September 1992

Operated by Universities Research Association Inc. under Contract No. DE-AC02-76CHO3000 with the United States Department of Energy

Disclaimer

MUSIM
Program to Simulate Production and Transport of Muons in Bulk Matter

A. Van Ginneken
Fermi National Accelerator Laboratory*
P. O. Box 500, Batavia, IL 60510

September 1992

Abstract

The Monte Carlo program MUSIM simulates production of muons in high energy hadronic and electromagnetic showers and their subsequent transport through bulk matter. The energy range includes the SSC/LHC regime. The program is briefly described and some results are shown.

1 Introduction

While hadron shielding requirements increase roughly logarithmically with energy, the increase in muon shielding is closer to linear. This has considerable impact on siting criteria, etc., for LHC, SSC and any multi-TeV accelerators contemplated for the more distant future. *Calculation* of muon shielding also gets more complicated at higher energies. 'Prompt' μs, i.e., other than from π and K decay, play an increasingly important role. These come from a variety of sources including some from electromagnetic showers. Mechanisms and cross sections associated with these sources are not universally agreed upon but they can nonetheless contribute significantly to μ flux or dose in a given problem. Whereas muons from π/K decay follow directly from the particle production model used to simulate hadron cascades,

*Work supported by the U.S. Department of Energy under contract No. DE-AC02-76CHO3000.

prompt μ generators must be put expressly into the program. Multi-TeV μ transport also gets more complicated. Sub-TeV muons lose energy predominantly by ionization which is subject to only minor fluctuations. For a typical muon produced in a cascade these fluctuations—governed by the Landau distribution—are negligible compared to the energy distribution at production. Above ~ 1 TeV pair production and bremsstrahlung gain increasing importance as do the much larger fluctuations associated with these processes. The effects of this are illustrated in ref.[1] which presents some graphs of muon range distributions in the 0.01 to 20 TeV energy domain. The spread in range grows with energy and at the higher energies becomes comparable to its average value. Dose distribution as a function of distance along the trajectory of a multi-TeV μ is thus strongly affected by these fluctuations which should therefore be included in the simulation. This phenomenon also spoils the approximation, often used in deep penetration problems, that only first generation muons need be considered. While muons from later generations certainly have lower average energy, they are also more numerous and it is not clear—after folding in the fluctuations—at what point they can be neglected.

In the past muon shielding problems at Fermilab have been addressed using a special version of the Monte Carlo code CASIM.[2] This version—referred to as CASIMU—consists of CASIM supplemented by μ production via π/K decay plus a prompt component described by an empirical formula which gives the ratio of prompts to πs produced as a function of Feynman-x ($x_F \equiv p_z^{CM}/p_{z,max}^{CM}$).[3] Thus, in a CASIMU Monte Carlo, every π produced is also a prompt μ but weighted down as per ref.[3]. Predictions of this program agree reasonably well with a number of observations.[4]

With the advent of a better understanding of prompt muons, an *ab initio* attempt to calculate production from these sources seems worth undertaking primarily to offer more confident extrapolation to multi-TeV energies. This is the basic objective of the new code—called MUSIM—described in this note. The prime requisite of the prompt μ production models is that they compare reasonably well with data and remain physically reasonable when extrapolated to multi-TeV energies. A large measure of convenience also enters into this since these models must be translated into efficient Monte Carlo algorithms for use in MUSIM. Under the circumstances it may be tempting to use a somewhat broader brush and combine some of these sources, i.e., aim somewhere between CASIMU—which lumps together all prompts—and MUSIM where each source is treated individually. This would simplify the program and might speed up execution some. But the present

approach makes MUSIM easier to update with new data, predictions from event generators, etc. Also in some applications one may wish to replace certain production cross sections with estimated upper or lower limits—or simply identify each component of the dose—to gain a better understanding of the uncertainties associated with MUSIM results.

It should be noted that MUSIM—as well as CASIM which is a part of it—does not simulate complete events but uses extensive weighting to estimate muon dose or flux *averaged over a large number of incident particles.* Thus MUSIM does not predict shower-to-shower fluctuations in the number of muons produced in any particular region of phase space—it predicts averages. This *modus operandi* has great computational advantages whenever event-by-event fluctuations don't matter. It should be recognized, however, that MUSIM does not merely do away with *all* fluctuations. There are types of fluctuations, e.g., those mentioned above associated with μ energy loss, which influence even the averaged results and hence must be included.

For most applications, the more energetic muons are also the more interesting. Therefore μs generated in MUSIM are biased towards higher energy, in roughly linear fashion. Such a bias aims in a general way at expediting a typical calculation but is obviously not optimal for each particular problem and may occasionally need modification to yield useful results in reasonable CPU times. Both the particles selected to participate in the hadron and electromagnetic cascade [5] and the muons generated by them are chosen with such a bias. This bias may take the form of muon 'splitting' (see sec. 2.1).

Below, sec. 2 specifies the assumptions regarding the various μ sources. Sec. 3 contains a brief description of μ transport. Sec. 4 presents a few MUSIM results including a limited comparison with CASIMU. Concluding remarks are in sec. 5. Refs.[6] include brief summaries of a preliminary version of MUSIM.

2 Muon Sources

In the context of this work, μ production falls conveniently into three groups: (1) π/K decays, and prompt muons originating from (2) hadronic or (3) electromagnetic showers. Part (2) may be subdivided into muons from meson decay and from the continuuum. There is nothing basic about this division, e.g., parts of (2) and (3) arise from decay of the same short lived particles. There are still large uncertainties attached to prompt μ production, particularly in the TeV regime were very little data exists. The Tevatron and

CERN colliders easily surpass SSC fixed target energies but data are sparse, limited to high p_T, and do not include nuclear targets. However, results and experience derived from these machines tend to rule out that any big surprises are in store for SSC/LHC fixed target muon shielding.

2.1 π/K Decay

As mentioned in sec. 1, π/K decay muon production follows directly from the production model used to simulate hadron cascades.[7] In MUSIM below 1 TeV this is the Hagedorn-Ranft model.[8] Above 1 TeV simple empirical formulae,[9] based on existing collider data and theoretical predictions, are used. For multi-TeV colliding beams a simple model [1] is available for use in the code, also in the form of inclusive distributions. Alternatively, one may use one of various available Monte Carlo event generators [10] for colliding beams and treat subsequent collisions and μ transport via MUSIM.

To generate an adequate sample of decay muons, every π produced is assumed to decay into one or more μs—appropriately weighted for decay probability and μ-splitting. When a π/K decay muon is split, a number of identical copies are produced with equispaced azimuthal decay angles and then traced separately through the problem geometry. The number of copies is never less than unity and is determined from the π's weight, energy, and direction. Because CASIM does not calculate Ks explicitly, πs also serve as generators for K-decay μs: a CASIM produced π is assumed to be 90% π and 10% K of equal momentum. Muons are generated using K-decay lifetime, branching ratios, and kinematics. Here also one or more K-decay muons are produced per π created in the calculation.

Hyperons provide a decay muon source similar to π/K but, since both production cross sections and branching ratios into μs are much smaller than for π/K, they may be neglected.

2.2 Prompt–Mesons

Hadronically produced prompt muons in MUSIM include those derived from decay of D, η, and several types of vector mesons. The list is far from exhaustive. However, for those omitted either the production cross section (e.g., B, Υ) or branching ratio (some lighter resonances) are too small to warrant inclusion at the present level of sensitivity. See also the comment below in sec. 2.2.2 on separation of continuum and meson produced dimuons.

2.2.1 D Mesons

At sufficiently high energies D mesons become a prolific source of prompt muons. Data for D production by protons on protons and nuclei are reported up to $\sqrt{s}$ of about 60 GeV from CERN ISR data, though there is strong disagreement among different experiments in this energy regime.[11] For π^- there is a smaller sample of data available while very little data exist for π^+. Theoretical predictions are strongly parameter dependent but by and large reproduce observation.[12]

Total Cross Section. The total cross section in μbarn for D production (all charge states, $x_F > 0$) for NN and πN collisions (N stands for nucleon—p or n) is assumed to be

$$\begin{aligned} \sigma &= 2\sqrt{s} - 30 \qquad \sqrt{s} \leq 50 \\ &= 50 \ln \sqrt{s} - 125 \qquad \sqrt{s} \geq 50 \end{aligned} \tag{1}$$

where $\sqrt{s}$ is in GeV and $\sigma = 0$ below $\sqrt{s} = 15\,\text{GeV}$. This reproduces lower energy data reasonably well and agrees closely with a calculated result at $\sqrt{s}$ of 630 GeV.[13] Assuming the same values to hold for πN and NN agrees with most—but not all—observations. This assumption entails that $\sigma_{x_F<0} = \sigma_{x_F>0}$ for πN as well as NN.

Differential Cross Section. For both N and π projectiles the form

$$\frac{d\sigma}{dp_T^2\, dx_F} = k \cdot (1 - |x_F|)^n \cdot \left(e^{-ap_T^2} + b\sqrt{s}e^{-cp_T^2}\right) \tag{2}$$

is assumed, with k fixed by normalization. A value of $a = 1.2\,(Gev/c)^{-2}$ is close to most measurements at low p_T, low $\sqrt{s}$. The second exponential introduces a slow rise in average p_T with $\sqrt{s}$ which flattens out when $\langle p_T \rangle$ approaches m_D (by choice of parameter c). Such a rise is not clearly indicated by the data but appears more certain in J/ψ production although it is not uniquely quantified even there. Values of $b = 0.001$, $c = 0.3$ are in general agreement with J/ψ data [14] and are also adopted for the Ds. For $x_F \geq 0$, $n = 5.5$ for NN and $n = 3.5$ for πN are consistent with most observations though there is considerable disagreement among them. For $x_F \leq 0$, $n = 5.5$ is assumed in both cases. This means that $d\sigma/dx_F$ is discontinuous at $x_F = 0$ for πN, which is tolerated for simplicity. No attempt is made to distinguish between D charge states in the differential cross section.

A Dependence. The A-dependence is, as is customary, parametrized by an A^α factor. Here an overall factor, with $\alpha = 1$, is adopted. This value of α is in accord with the more recent data and with the premise that Ds are produced in hard collisions. In more refined models α may depend on x_F and p_T.

Decay. D mesons have zero spin and decay isotropically with a muon energy spectrum following the usual beta decay phase space. The branching ratio to 'μ+anything' averaged over D^0 and $D^\pm$ is assumed to be 13.5%.[15] There exist a number of such branches with $K(n\pi)\mu\nu$, $n = 0, 1, \ldots$, being the most prominent and with K occasionally replaced by K^* with $m_{K^*} =$ 892 MeV. Specific branching ratios are known only with large error bars. For simplicity, D decays are assumed to be equally distributed between $K\mu\nu$ and $K^*\mu\nu$.

2.2.2 Vector Mesons and η

Vector mesons, and the (J=0) η, η' mesons, are produced in greater abundance than Ds in hadronic collisions but their decays generate far fewer muons. The $\mu^+\mu^-$ decay branch of $\rho + \omega$ and of J/ψ appear as prominent peaks above a background from which they are readily separated. Others contribute significantly but are less clearly resolved. In MUSIM $\phi \to \mu^+\mu^-$, $\eta(\eta') \to \mu^+\mu^-\gamma$, and $\omega \to \mu^+\mu^-\pi^0$ are included. Data on production of these mesons is rather sparse particularly if one is interested in the complete phase space or even just the part where production is largest. For the lighter species, branching ratios into muons (of order 10^{-4}) have fairly large errors attached.

Since each decay here involves two muons, care must be taken in separating this component from the dimuon continuum to avoid double counting. The continuum description in MUSIM (see below) is largely empirical and consists of what remains after the other sources are removed. A dimuon source not explicitly included is thus not outright neglected but becomes part of the continuum, though an error is incurred to the extent that angular distributions, energy scaling, etc., differ between these sources and the continuum.[16]

In production and decay kinematics, *average* values are used for the meson masses since widths are typically small compared to the average. The ρ is somewhat of an exception to this though neglecting its width is unlikely to seriously affect MUSIM results.

Total Cross Section. In the high energy limit total cross sections for these sources are assumed to be proportional to the average total (charged) multiplicity, specifically as parametrized by Thomé et al.[17]

$$\langle n_{ch} \rangle = 0.88 + 0.44 \ln s + 0.118 (\ln s)^2 \tag{3}$$

with s expressed in GeV^2. For both NN and πN the proportionality constants κ_i $(= \sigma_i / \langle n_{ch} \rangle)$, listed in Table I in units of $m$barn, are adopted from an informal survey of available data with most weight attached to high energy experiments which are sensitive to low p_T.[18] The η and $\eta\prime$ are assumed to be produced in equal amounts [19] as are ρ and ω. Eq.(3) is multiplied by an approach-to-scaling factor

$$f_{ap} = (1 - \sqrt{s_i}/\sqrt{s})^q \tag{4}$$

where $\sqrt{s_i} = 2.5$ GeV and $q = 1/2$ for the lighter mesons while $\sqrt{s_i} = 5$ GeV and $q_N = 12.0$, $q_\pi = 7.3$ for J/ψ.[14] Eq.(3) along with the entries of Table I refer to production for $x_F > 0$. For incident π the backward hemisphere is parametrized the same as $x_F > 0$ for incident N.

Table I *Meson Production Parameters*

		κ	n
$\eta + \eta\prime$	N	0.6	2.5
	π	0.85	1.0
$\rho + \omega$	N	1.0	3.5
	π	1.3	1.5
ϕ	N	0.05	5.0
	π	0.06	3.0
J/ψ	N	$2.2\,10^{-6}$	5.0
	π	$1.5\,10^{-6}$	3.0

Differential Cross Section. For J/ψ eq.(2) is used, with n according to Table I. For the lighter species

$$\frac{d\sigma}{dp_T^2\, dx_F} = k \cdot (1 - |x_F|)^n \cdot \left(e^{-3.4 p_T^2} + 0.1 e^{-p_T^2/m_R^2} \right) \tag{5}$$

with m_R the meson mass in GeV and the ns from Table I. The ns and κs of Table I derive from fits reported in the literature along with some made expressly for this study.[20] The second term of the p_T factor is not very well quantified although omitting it would certainly underestimate production at large p_T. For each case, k normalizes eq.(5) to the total cross section.

A Dependence. As with D production, the total cross section is multiplied by A^{α}. In MUSIM $\alpha = 2/3$ is assumed for η, ρ, ω, and ϕ while $\alpha = 1$ for J/ψ.[21] Though somewhat less certain, a nuclear target dependence appears to be present also in the *differential* cross section with α increasing with p_T and decreasing with x_F. This is not included in the MUSIM parametrization.

Decay. The μ branching ratios are averages taken from ref.[15] and are listed in Table II. For η and $\eta\prime$ only $\mu\mu\gamma$ is assumed present. Other branches leading to muons are much smaller. For ω both $\mu\mu$ and $\mu\mu\pi^0$ are included. For J/ψ the relatively large branch into μs compensates somewhat for the much smaller production cross section.

Table II *Meson Branching Ratios into* μ

Meson	Product	BR
ρ	$\mu\mu$	$4.6\,10^{-5}$
η	$\mu\mu\gamma$	$3.1\,10^{-4}$
$\eta\prime$	$\mu\mu\gamma$	$1.1\,10^{-4}$
ω	$\mu\mu$	$7.1\,10^{-5}$
	$\mu\mu\pi^0$	$9.6\,10^{-5}$
ϕ	$\mu\mu$	$2.5\,10^{-4}$
J/ψ	$\mu\mu$	$6.9\,10^{-2}$

Since η has zero spin the angular distribution for $\eta \rightarrow \mu\mu$ is isotropic. For the spin-one vector mesons this holds to good approximation.[22, 23] Three body decays are treated in two stages. First the resonance decays—isotropically—into a γ, or π^0, and a muon pair with invariant mass distribution from theoretical predictions [24] with experimentally determined form factors.[25] The latter then decays—also isotropically—into two muons. For convenience, the $\mu\mu$ mass is chosen from empirical formulae which approximate those from refs.[24].

2.3 Prompt–Continuum

The continuum refers to dimuons which are not decay products of a particle or resonance. For $\mu\mu$ with large invariant mass the dominant continuum component is the Drell-Yan process. But it appears that for pairs emitted with low invariant mass neither Drell-Yan nor resonance decay can account for what is observed experimentally—although there are claims to the contrary.[26] A plausible mechanism to produce these muons is soft

annihilation[27], i.e., $q\bar{q} \rightarrow \mu\mu$ where q and $\bar{q}$ are *produced* in the collision as opposed to being brought in by the incident particles as in Drell-Yan. There are other theories [28] and other ways of calculating the excess low mass muon pairs which are based more or less on the same idea.[29]

2.3.1 Low Mass Continuum

It is assumed here that the low mass continuum is entirely due to soft annihilation, although it is possible that more than one mechanism contributes significantly. As mentioned in sec. 2.2.2, the low mass continuum in MUSIM includes what remains after subtracting out the other MUSIM sources. This procedure relies mainly on the Chicago-Princeton data.[22, 23] In principle, at least, for that energy regime (150–225 GeV) and target mass (A=9 and 12) everything should thus be accounted for. But even if the soft annihilation picture is the correct one, the scaling procedures adopted here cannot claim to be very well supported. Data are rather sparse and sometimes contradictory. Serious calculation of this effect requires detailed understanding of the spacetime development of hadronic collisions and—questions of validity aside—most models for this tend to be rather complicated.[30]

Total Cross Section. For fixed incident energy the soft annihilation model predicts a faster than linear increase of dilepton production with multiplicity on an event-by-event basis. At $\sqrt{s} = 63$ GeV, ref.[31] presents

$$R = -0.20 + 0.069 n_{ch} + 0.0044 n_{ch}^2 \tag{6}$$

as a fit to more detailed calculation, where $R = 10^4 \sigma_{\ell^+\ell^-}/\sigma_{had}$ averaged over all events with the same charged particle multiplicity, n_{ch}. Such an effect is observed—though not quantitatively verified—in e^+e^- production at the ISR.[32] Here it is assumed that, *averaged over all events*, $\mu^+\mu^-$ production varies with *average* multiplicity in a manner similar to eq.(6)

$$\sigma_{\mu^+\mu^-} = 0.5 \left(\langle n_{ch} \rangle + 0.06 \langle n_{ch} \rangle^2 \right) \tag{7}$$

where $\sigma_{\mu^+\mu^-}$ is expressed in μbarn. In effect, eq.(7) describes the energy dependence of the total cross section. It is assumed to hold for both NN and πN collisions, with $\langle n_{ch} \rangle$ again according to eq.(3). The mass spectrum of the continuum is described by

$$P(M) = kM^{-1} \left(1 - 4m_\mu^2/M^2 \right)^{1/2} e^{-3M} \tag{8}$$

based mostly on refs.[22, 23] with k providing normalization.

Differential Cross Section. Parametrization of the differential cross section also relies on the Chicago-Princeton data:

$$\frac{d^3\sigma}{dx_F\,dp_T^2} = k \cdot (1 - x_F)^c \cdot \left(e^{-8m_T^2} + 0.04e^{-1.6m_T^2}\right) \tag{9}$$

where for incident nucleons $c = 8.0$ when $M \leq 0.45\,\mathrm{GeV}$ and $c = 5.0$ for larger masses. Corresponding values for incident pions are $c = 5.0$ and $c = 3.0$, while k ensures normalization so that eq.(9) integrates out to eq.(7).

A Dependence. Dependence on target nucleus enters again as an A^α factor which multiplies the total cross section, with $\alpha_p = 0.68$ and $\alpha_\pi = 0.80$ taken from experiment.[33, 34] No strong dependence of α on x_F is seen.

Angular Distribution. In the $\mu\mu$ restframe the angular distribution of the μs is assumed to be isotropic. At most small deviations from this are observed.[22, 23, 35]

2.3.2 Drell-Yan

In contrast to the low mass region, Drell-Yan [36] μ production is reasonably well understood. Much of what is needed here is summarized in reviews of the subject.[34, 37, 38] For $M_{\mu\mu} <\sim 3 - 4\,\mathrm{GeV}$, Drell-Yan production falls well below other sources and emphasis is therefore on the high mass region. A more accurate prescription than what follows is possible in terms of structure functions of the collision partners. However, in a typical problem Drell-Yan contributes very little and hence does not warrant the extra complication.

Total Cross Section. Simple Drell-Yan scaling predicts that for a given projectile and target $M^3 d\sigma/dM$ depends only on the scaling variable $\tau = M^2/s$. For large M, this is more or less observed experimentally. The cross section depends strongly on target and projectile species according to which types of valence quarks are brought into play. An exponential form of the scaling function is assumed:

$$M^3 d\sigma/dM = k\left(e^{-B\sqrt{\tau}} + Ce^{-B_0\sqrt{\tau}}\right) \tag{10}$$

where $k_N = k_\pi = 40\,nb \cdot GeV^2$ per nucleon ($x_F > 0$), while $B_N = 13$, $B_{\pi^+} = 9.5$, and $B_{\pi^-} = B_0 = 8$. In the second term $C_N = 0$, $C_{\pi^+} = 0.25$,

and $C_{\pi^-} = 1$ ensure that (for nuclear targets) predicted and observed π^+/π^- cross section ratios at high mass are reasonably well reproduced in MUSIM.

Differential Cross Section. The differential cross section is assumed to have the familiar form

$$\frac{d^3\sigma}{dx_F dp_T^2} = k \cdot (1 - x_F)^c \cdot e^{-p_T^2/B} \tag{11}$$

where k enforces normalization as per eq.(10), $c_N = 3.8$ and $c_\pi = 1.8$ (but $c = 0$ for $x_F < 0.1$ in both cases), and $B = 0.26 + 0.029\sqrt{s} + 0.00080s$.

A Dependence. In accordance with Drell-Yan being a hard process an overall linear A dependence is assumed. This is consistent with experiment.

Angular Distribution. In the $\mu\mu$ restframe the angular distribution is assumed to follow $(1 + cos^2\theta)$, in agreement with observation and theoretical expectation.

2.4 Electromagnetic

Photons—produced in hadronic showers by π^0 decay and regenerated in electromagnetic showers via bremsstrahlung—can create μs as Bethe-Heitler pairs. In addition, the photon has $J = 1$ and can therefore transform diffractively into a vector meson and thence into a muon pair. On a nuclear target this can proceed via three different mechanisms: coherent, incoherent, and inelastic. For *coherent* production the entire nucleus remains intact while the photon transforms into a vector meson, with only a tiny amount of energy lost on nuclear recoil. *Incoherent* production refers to the same process off an individual nucleon within the nucleus, with the nucleon being ejected in the process. The energy spent on this now includes some binding energy but is again minimal. An *inelastically* produced vector meson is accompanied by other mesons which may share a large fraction of the energy. This leads to vector mesons (and hence to μs) much like those produced in hadronic collisions but with much lower cross section and they are therefore neglected. The same applies to photo- *vs* hadroproduction of D-mesons. Vector meson production via virtual photons (inelastic $e^\pm$ scattering) is likewise neglected since—in a thick target—this will everywhere be much smaller than production by real photons. Annihilation of e^+, which are copiously produced

in $e\gamma$ showers, with atomic electrons can also yield a muon pair. These are the electromagnetic muon generators included here. While there are some omissions, these are unlikely to be of any importance in MUSIM applications.

Cross sections for electromagnetic muon production are typically much smaller than for the hadronic modes. They may nonetheless contribute significantly since (1) with increasing energy an increasing fraction of the energy of a hadron initiated shower is spent on $e\gamma$ showers, and (2) for most muon production in an $e\gamma$ shower, almost the entire energy of the γ (or e^+) converts into energy of the $\mu\mu$ pair (in contrast to hadronically produced muons).

2.4.1 Bethe-Heitler

Simulation of electromagnetic showers within CASIM is done via subprogram AEGIS [39] which includes bremsstrahlung and e^+e^- production. AEGIS also uses extensive weighting with only one particle per shower generation being tracked, (γ, e^+, or e^-). When energetically possible, muon pair production is expected to occur at a rate of $(m_e/m_\mu)^2$ times that for e^+e^-, neglecting differences in avaiable phase space—which disappear quickly with increasing energy. The MUSIM algorithm simply assumes that every n^{th} pair produced ($n \approx 10$ seems a good choice) is a $\mu\mu$ with weight $n(m_e/m_\mu)^2$. Specifically, an $e^+(e^-)$ becomes a $\mu^+(\mu^-)$ with the same total energy—if kinematically permissible—and with the same direction of motion.

2.4.2 Vector Mesons

The $\gamma p \rightarrow Vp$ total cross sections and slope parameters, b, of the t dependence (in $d\sigma/dt \propto e^{bt}$) for $V = \rho, \omega, \phi$, and J/ψ are taken from ref.[40]. Assuming these to hold also for $\gamma n \rightarrow Vn$, Glauber theory predicts coherent and incoherent cross sections for nuclear targets.[41] For coherent production this involves an integral over impact parameter which makes it ill suited for direct Monte Carlo sampling. These cross section are therefore pretabulated for each material present in the problem. For the incoherent cross section, the nuclear $d\sigma/dt$ is taken as $d\sigma/dt$ for $\gamma p \rightarrow Vp$ scaled up by an 'effective number' of nucleons.[41] Decay parameters of the vector mesons are as listed for hadroproduction.

2.4.3 Positron Annihilation

Positrons generated in $e\gamma$ showers can annihilate with atomic e^-s into a muon pair which carries off all the energy of the e^+. The cross section for this process is taken as $87/s$ nb per electron, where s is in GeV^2 and the angular distribution follows a $(1 + cos^2\theta)$ law at sufficiently high energies (see, e.g., ref.[15]).

3 Muon Transport

A muon generated within a hadron- or $e\gamma$ shower is traced stepwise through the (user provided) problem geometry until it stops or exceeds some predetermined boundary. The usual processes which slow down the μs are taken into account: atomic excitation and ionization, direct e^+e^- production, bremsstrahlung, and nuclear interaction. These processes also cause some angular diffusion of the muons—strongly correlated with energy loss—which has important consequences in many applications. For a muon beam traversing a thick target radial growth is determined by this diffusion and its correlation with energy losses. This is also true to a large extent for the 'beam' composed of the more energetic muons produced in a hadron cascade.

For ionization losses a restricted energy loss ($\Delta E \leq 10$ MeV in an individual encounter—corresponding to $\sim$ 1.5 MeV per g·cm^{-2}) is applied *continuously* along the muon trajectory. The rest is treated as δ-rays on an event-by-event basis. In each step taken by the muon the number, n, of such events is determined and (if $n > 0$) for each event the energy loss is determined using Bhaba's formula.[42] Since this is essentially a two body process there exists a unique correlation between energy loss and angular deflection: $-t = 2m_e\Delta E \simeq p^2\theta^2$.

For the other processes energy and angle are not uniquely correlated and they are treated as outlined in ref.[43]. In each simulated event the energy loss is randomly chosen from an empirical probability distribution which depends on muon energy. From this energy loss, and dependent upon incident muon energy and (in some cases) target Z and A, the *rms* angle of deflection, θ_{rms}, follows from another empirical formula. A particular angle for the event is then randomly chosen from a Gaussian with zero mean and rms angle equal to θ_{rms}. Even though angular distributions of individual events are known to be decidedly non-Gaussian, this procedure is justified in a way entirely similar to the use of Gaussians in multiple scattering.

As mentioned in sec. 2.1, π and K decay are always assumed to create—at least—one (weighted) μ, regardless of the length of the trajectory. The point at which the muon is created is chosen with exponentially declining probability along the π/K trajectory.[44] In MUSIM muons are split according to energy and angle with much of the treatment easily adapted to the problem at hand.

4 Results

A few results obtained with MUSIM are included here. The more generally useful results tend to pertain to simple geometries which then provide a convenient platform from which to launch more complicated ventures. In ref.[1] penetration of a monoenergetic muon pencil beam in homogeneous soil is analyzed for various μ energies. This is a problem entirely determined by muon transport and the results there are obtained with essentially the same code as appears in MUSIM.[45] An interesting case of general interest which does include μ *production*—and thus reflects what's new in MUSIM—is that of muon dose due to a monoenergetic proton (pencil) beam incident on homogeneous soil. This is the zeroth order approximation to muon dose behind a beam dump or target, i.e., the dump or target assembly and surrounding structures are replaced by more soil. Results, for a selection of incident energies, are presented in the form of isodose contour maps in units of *rad* per incident proton as a function of radius and distance measured along the beam direction. Using the standard 2 MeV/g·cm^{-2} the dose is convertible to an approximate muon fluence. Hadron dose is excluded from these results.

Figs. 1–5 show muon isodose contours in soil (of density 2.24 $g \cdot cm^{-3}$) for incident protons in the range 0.1–20 TeV as calculated with MUSIM. Figs. 6–8 display CASIMU results for 100, 300, and 1000 GeV, which compare directly to figs. 1–3. For all these graphs contours of 10^{-23} *rad*/inc.proton and below are omitted for lack of statistical accuracy. At very low z and r some contours may be missing for lack of spatial resolution, particularly at the higher energies. Not unexpectedly, differences between the two calculations increase with energy as the prompts gain in relative importance. Agreement between the two programs in the Fermilab regime is good though not surprising since π/K decay dominates there. Although more detailed comparisons may be desirable, it seems fair to expect agreement of MUSIM with observations to be comparable to what is attained with CASIMU.[4] The 20 TeV result (fig. 5) may be compared with that of CASIMU presented in fig. 102

of ref.[1]. Though the discrepancy is widening with energy, results are still quite similar.[46] There is noticeably less penetration along the z axis with MUSIM. The largest difference appears to be at lower z and larger radius where muon dose appears to be larger for MUSIM.[47] This probably reflects larger p_T of produced muons for which Ds and soft annihilation appear to be mainly responsible. This trend is already discernable at the lower energies.

Fig. 9 shows radially integrated energy deposition as a function of longitudinal distance along the beam for 20 TeV protons incident on a homogeneous soil target as calculated by MUSIM and sorted by mechanism as described in sec. 2. Fig. 10 is the corresponding longitudinally integrated energy deposition as a function of radius. At large radii, and also at large longitudinal distances, soft annihilation appears to be the largest component. It is unfortunate that this component is not very well understood and that thereby the calculation as a whole acquires a large margin of error. However, it should be noted that, in this regard, the case of 20 TeV protons on a solid target is close to a 'worst case' and this conclusion therefore does not cast the same uncertainty on *all* MUSIM results. At lower energies and/or for geometries with large evacuated regions, π/K decay will be relatively more important and so less uncertainty will be associated with total muon dose. Nonetheless, the implication that soft annihilation muons play an important role in shielding matters suggests that this component be examined more closely with an eye towards improving its description in MUSIM.

By contrast, and strictly by way of illustration, fig. 11 pertains to a more specific geometry. To simulate—in approximate fashion—one beam loss scenario in LHC, a continuous dipole is placed in a circular tunnel with radius equivalent to that of LEP/LHC and with the magnetic field adjusted to an 8 TeV proton orbit. In this case, beam is lost at a point ($z = 0$) on the *out*-side of the vacuum chamber, i.e., in the horizontal plane on the inner edge of the vacuum chamber, radially away from the center of the accelerator. (Whether loss is on the in-side or out-side of the vacuum chamber makes considerable difference in the decay path provided to the π/Ks and thus to the muon dose.) This specific result is from a forerunner of MUSIM [6] and the muon dose contours are in units of *sievert* per proton lost.

5 Concluding Remarks

An interesting facet of μ shielding is the competition between prompt and decay components. This is strongly dependent on many variables: incident energy, geometry and material composition of the 'target', and on the presence of magnetic fields. The decay lengths for π and K increase almost linearly with energy thus making the prompts relatively more important. In a homogeneous medium the decay component will increase almost linearly with nuclear interaction length (expressed as a *distance*). In more complicated surroundings the geometry must be modeled with some care. As in the example of fig. 11, when beam is lost inside an accelerator the magnet aperture may offer the π/Ks a long decay path. This is also the case, e.g., in straight sections with few magnets or other apparatus present and in regions of low density within a magnet. Magnetic fields also affect this prompt *vs* decay competition. Muons are well known to exhibit oscillations, i.e., after being swept out of the aperture they may be bumped back into it by the return field of a dipole, often completing many such cycles. In principle this can all be simulated since the geometry and magnetic fields—including the return field—can be modeled to any desired accuracy. In practice one often foregoes such detailed simulations in favor of 'sample' calculations which offer only order-of-magnitude estimates but can be completed and analyzed in a reasonable time frame. Often there are enough other uncertainties attached to modeling such problems: beam loss, questions of alignment, etc., to discourage the pursuit of ultra-realism in these simulations. The example of fig. 11 may be called a sample calculation since it is a considerable simplification of what a realistic LHC beam loss is expected to be like.

There is a tendency in applications of this kind to deliberately overestimate any relevant, but poorly known, cross sections or other parameters in order to arrive eventually at conservative muon dose predictions. This tendency is resisted here. The user might therefore consider applying a safety factor to MUSIM radiation dose estimates, particularly if there are legal ramifications and if no other safety factors are implied, e.g., in beam loss assumptions or simplifications of the geometry. In many such cases one will, for lack of more precise information, formulate 'worst case' assumptions at this level and thus obtain conservative dose rate estimates. But this is properly at the disposal of the user—who must supply such information to the program anyway—while MUSIM aims to remain free of any such deliberate bias.

In connection with radiation dose, etc., it is important to bear in mind

that muons—unlike neutrons—eventually do 'range out'. This means that muon dose must be zero beyond a certain envelope. Fluctuations in energy loss extend, but do not remove, this envelope since restricted collision losses are always present and are nearly continuous. Therefore, within the envelope but near its boundary, the isodose contours (of the type shown in figs. 1–8, but continued to lower doses) will be crowded together. This puts an extra burden on the calculation: even minor changes in the model may cause huge changes in dose prediction in the vicinity of the envelope. Good statistics may be hard to come by since, in addition to coping with the diminished muon flux, one needs also increased spatial resolution to cope with the crowding of the contours. (As noted in sec. 4, for doses below about 10^{-22} *rad*/inc.proton the present calculations begin to suffer in this regard.) This has obvious implications for the safety analysis, most importantly that results should not be taken literally in this region.

The excess muons observed in cosmic ray showers associated with certain stellar sources should at least be mentioned in the present context.[48] While first observed almost a decade ago, it is still surrounded by controversy. A number of explanations involving new physics and/or new particles have been offered. At present it would be premature to include any of it in this work. The primaries are almost certainly not protons and the energies usually mentioned in this connection are well above those of the contemplated colliders. Nonetheless, this situation is worth monitoring and, if observations persist, some impact on future accelerators—particularly from μs produced by colliding beams—cannot be ruled out.

Acknowledgement. My thanks to Tom Kobilarcik for valuable scrutiny of the code while adapting it to UNIX.

References

[1] A. Van Ginneken, P. Yurista, and C. Yamaguchi, Fermilab Report FN-447/ssc-106 (1987).

[2] A. Van Ginneken, Fermilab Report FN-272 (1975).

[3] J. L. Ritchie et al., Phys. Rev. Lett. **44**, 230 (1980). In the earliest version of CASIMU [Fermilab TM-630 (1975)] prompt μs were taken as a constant fraction of π production. This was replaced by a simple linear dependence on x_F. Muon transport started out by referencing a range-energy table and was later converted to the present algorithm.

[4] J. D. Cossairt, et al., Nucl. Inst. Meth. **A276**, 78 (1989); J. D. Cossairt, A. J. Elwyn, and W. S. Freeman, Nucl. Inst. Meth. **A276**, 86 (1989).

[5] In CASIM the participants in the cascade or *propagating* particles are routinely chosen with a bias proportional to lab energy and are the only ones needed in MUSIM. *Recording* particles, used in hadron dose calculations, do not come into play here.

[6] *Radiological Considerations for the Environment around* LHC, G. R. Stevenson and R. H. Thomas, Eds., CERN-TIS/89-19-LHC Note 115 (1989); and *Super-Collider 3*, J. Nonte, Ed., p.1017, Plenum Press, New York (1991).

[7] From a strict computational view one has the freedom to adopt different models for cascade propagation and π/K muon generation though this would be hard to justify from a physics standpoint.

[8] R. Hagedorn, Suppl. Nuovo Cim., **3**, 147 (1965); R. Hagedorn and J. Ranft, Suppl. Nuovo Cim., **6**, 169 (1968).

[9] S. Qian and A. Van Ginneken, Fermilab Report FN-514 (1989)

[10] F. E. Paige and S. D. Protopopescu, BNL Report 38034 (1986); P. A. Aarnio, et al., CERN Report TIS-RP/168 (1986); H.-U. Bengtson and T. Sjostrand, Lund Univ. report, LU TP 87/3 (1987). It should be checked whether the main prompt muon sources are present in the generator or need to be added. The penalty for simulating full events for the original collision vis-a-vis inclusives is probably not prohibitive, though it may be worthwhile to introduce weightings to boost (energetic) muon generation.

[11] see, e.g., the compilations of S. P. K. Tavernier, Rep. Prog. Phys. **50**, 1439 (1987) and of M. F. Weber, Ph.D. Thesis, Univ. of Michigan (1988).

[12] see, e.g., R. K. Ellis, Fermilab Report Conf-89/168-T (1989).

[13] R. K. Ellis, Fermilab Report Conf-86/35-T (1986).

[14] V. Abramov et al., Fermilab Report Pub-91/62-E (1991).

[15] K. Hikasa et al., Phys. Rev. D **45**, 1 (1992).

[16] Double counting can occur also for mesons produced both directly and via decay of a heavier meson. At the present level of accuracy, this is not likely to be a big problem.

[17] W. Thomé et al., Nucl. Phys. **B129**, 365 (1977).

[18] M. Aguilar-Benitez et al., Z. Phys. C **44**, 531 (1989); N. M. Agababyan et al, Z. Phys. C **46**, 387 (1990); M. R. Atayan et al., Univ. of Nijmegen Report HEN-344/91 (1991); V. Abramov et al., Fermilab Report Pub-91/62-E (1991).

[19] This is based on 360 GeV $\pi^- p$ data of M. Aguilar-Benitez et al., Europhys. Lett. **4** 1261 (1987) which reports $\sigma(\eta) = 3.1\ mb$ for $x_F > 0.1$ versus $\sigma(\eta') = 2.9\ mb$ for $x_F > 0.3$. This suggests that overall $\sigma(\eta')$ is larger. However, at lower energies η' production appears to be much lower than η, see, e.g., N. H. Fuchs, Lett. Nuovo Cim. **20**, 103 (1977) and H. Kirk et al., Nucl. Phys. **B128**, 397 (1977).

[20] Note that the entries in Table I refer to $d\sigma/dx_F$ while some of the references parametrize $Ed^3\sigma/dp^3$.

[21] D. M. Alde et al., Phys. Rev. Lett. **66**, 133 (1991).

[22] K. J. Anderson et al., Phys. Rev. Lett. **37**, 799 (1976); G. G. Henry, Thesis, Univ. of Chicago (1978).

[23] J. G. Branson et al., Phys. Rev. Lett. **38**, 1331 (1977).

[24] R. H. Dalitz, Proc. Phys. Soc. (London) **A64**, 667 (1951); N. M. Kroll and W. Wada, Phys. Rev. **98**, 1355 (1955); C. H. Lai and C. Quigg, Fermilab Report FN-296 (1976).

[25] V. A. Viktorov et al., Sov. J. Nucl. Phys. **32**, 516 (1980).

[26] A. V. Bannikov et al., JINR (Dubna) Report E1-89-486 (1989).

[27] J. D. Bjorken and H. Weisberg, Phys. Rev. D **13**, 1405 (1976); V. Černý, P. Lichard, and J. Pišút, Phys. Rev. D **24**, 652 (1981).

[28] N. S. Craigie and D. Schildknecht, Nucl. Phys. **B118**, 311 (1977); T. Goldman, M. Duong-van, and R. Blankenbecler, Phys. Rev. D **12**, 619 (1979).

[29] E. V. Shuryak, Sov. J. Nucl. Phys. **28**, 408 (1978).

[30] P. Lichard, Z. Phys. C **37**, 125 (1987).

[31] V. Černý, P. Lichard, and J. Pišút, Z. Phys. C **31**, 163 (1981).

[32] V. Hedberg, Thesis, Lund Univ. (1987); T. Akesson et al., Phys. Lett. **192B**, 463 (1987).

[33] H. Cobbaert et al., Phys. Lett. **213B**, 395 (1988).

[34] R. Stroynowski, Phys. Rept. **71**, 1 (1981).

[35] B. Haber et al., Phys. Rev. D **22**, 2107 (1980).

[36] S. Drell and T. M. Yan, Phys. Rev. Lett. **25**, 316 (1970) and Ann. Phys. **66**, 578 (1971).

[37] I. R. Kenyon, Rep. Prog. Phys. **45**, 1261 (1982).

[38] C. Grosso-Pilcher and M. J. Shochet, Ann. Rev. Nucl. Sci. **36**, 1 (1986).

[39] A. Van Ginneken, Fermilab Report FN-309 (1978).

[40] Parameters for ρ, ω, and ϕ are from E. Paul, Proc. 1981 Int. Symp. on Lepton and Photon Interactions at High Energies, W. Pfeil, Ed., p. 301 (1981) while the J/ψs are from S. D. Holmes, W. Lee, and J. E. Wiss, Ann. Rev. Nucl. Sci. **35**, 397 (1985).

[41] K. S. Kölbig and B. Margolis, Nucl. Phys. **B6**, 85 (1968).

[42] B. Rossi, *High Energy Particles*, p.16, Prentice Hall, Englewood Cliffs, N.J. (1952).

[43] A. Van Ginneken, Nucl. Inst. Meth. **A251**, 21 (1986).

[44] The procedure for this is not obvious when strong fields or large angle scattering cause a π/K to follow a tortuous route. In MUSIM the decay probability in each π/K transport step is determined (and accumulated). To start, decay is assumed to take place within the first step—taken to be a straight line. Position and momentum vector of the π/K there are stored to later (possibly) generate a μ. The decay probability in the second step is then compared with that of the first and a random choice is made between the two on this basis. If the second step is selected, the appropriate coordinates and momentum replace the stored ones. Decay probability in the third step is compared with the *joint* probability of decay in the first two. If successful, the point of decay parameters in the third step replace the stored ones and so on at each successive step. Since, at high energy, the decay probability per step may be taken as constant, the procedure is computationally fast and easy. This procedure may be combined in various ways with muon splitting.

[45] The code TRAMU is essentially a subset of MUSIM which transports μs through arbitrary geometry.

[46] In ref.[1] the contours do not meet the z-axis properly. Since the contours may be continued to 'negative' radii (where they equal those on the positive domain) they must meet the z-axis at right angles.

[47] Because of compression of the z-scale at higher energies, any structure in the contours at low z becomes hard to resolve.

[48] see, e.g., F. Halzen, CERN Report TH-4570/86 (1986).

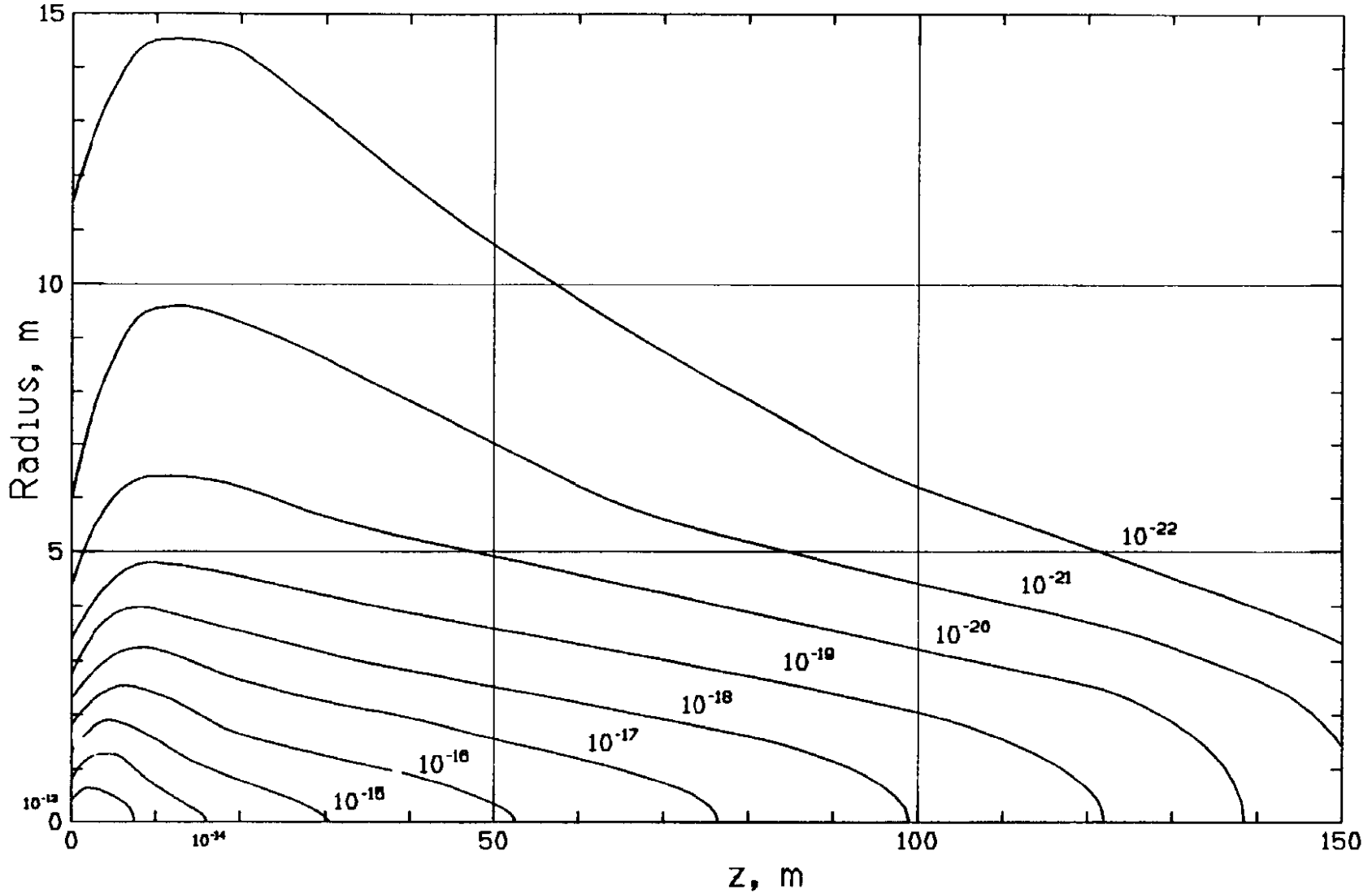

Fig. 1 Isodose contours due to muons in units of ***rad/inc.proton*** for 0.1 TeV protons incident on homogeneous soil as calculated by MUSIM program.

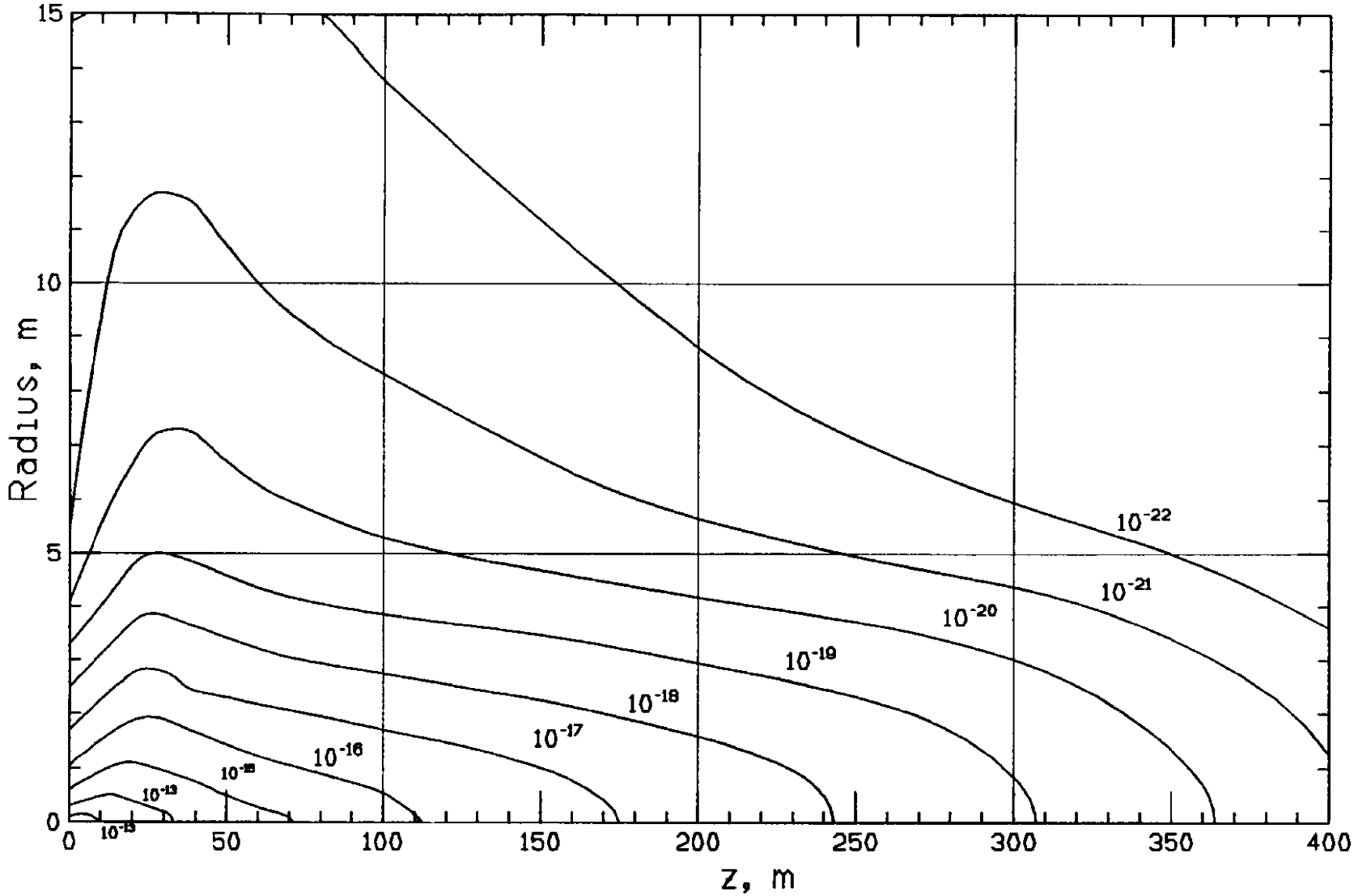

Fig. 2 Isodose contours due to muons in units of *rad/inc.proton* for 0.3 TeV protons incident on homogeneous soil as calculated by MUSIM program.

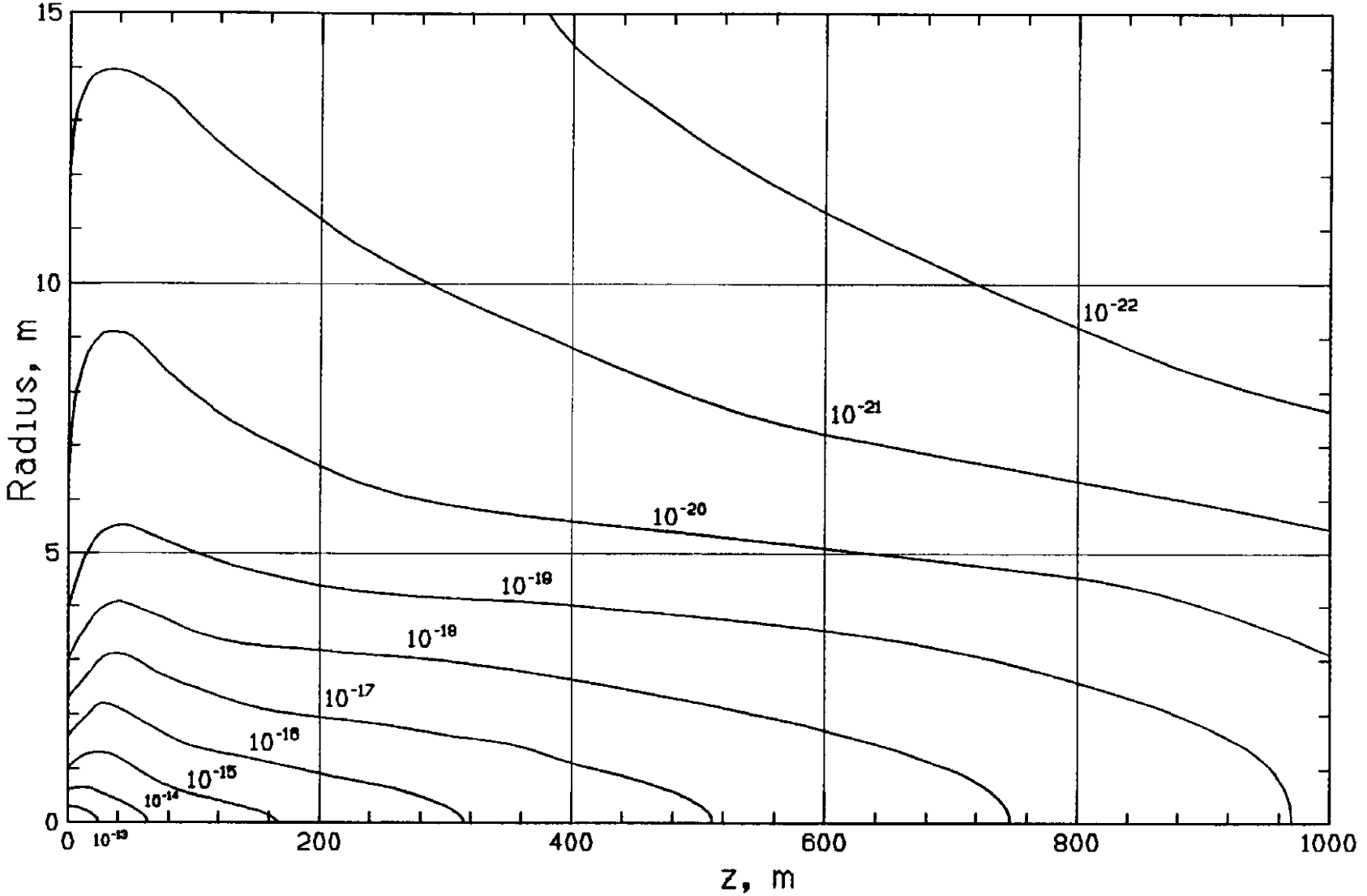

Fig. 3 Isodose contours due to muons in units of *rad/inc.proton* for 1 TeV protons incident on homogeneous soil as calculated by MUSIM program.

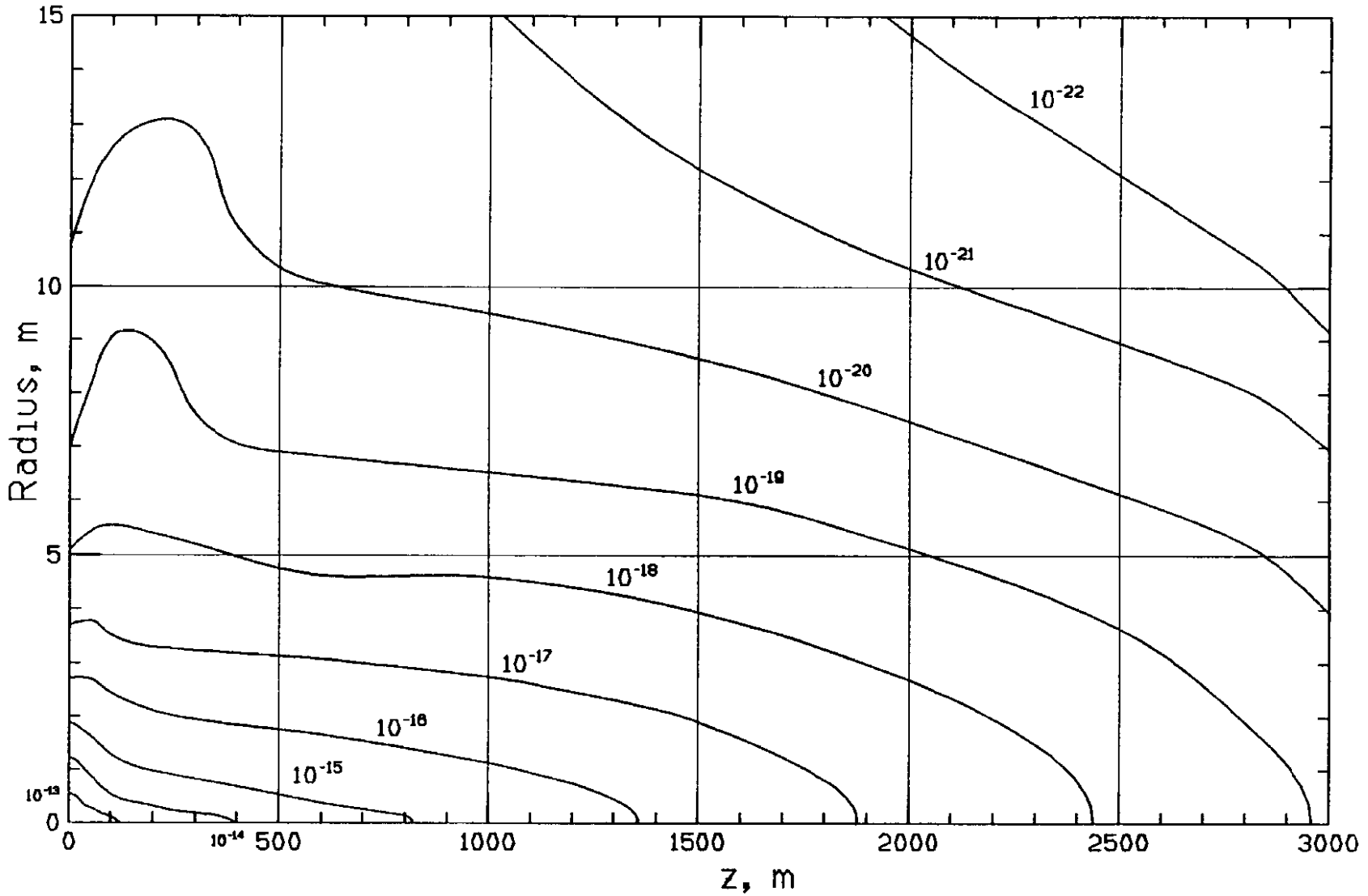

Fig. 4 Isodose contours due to muons in units of *rad/inc.proton* for 8 TeV protons incident on homogeneous soil as calculated by MUSIM program.

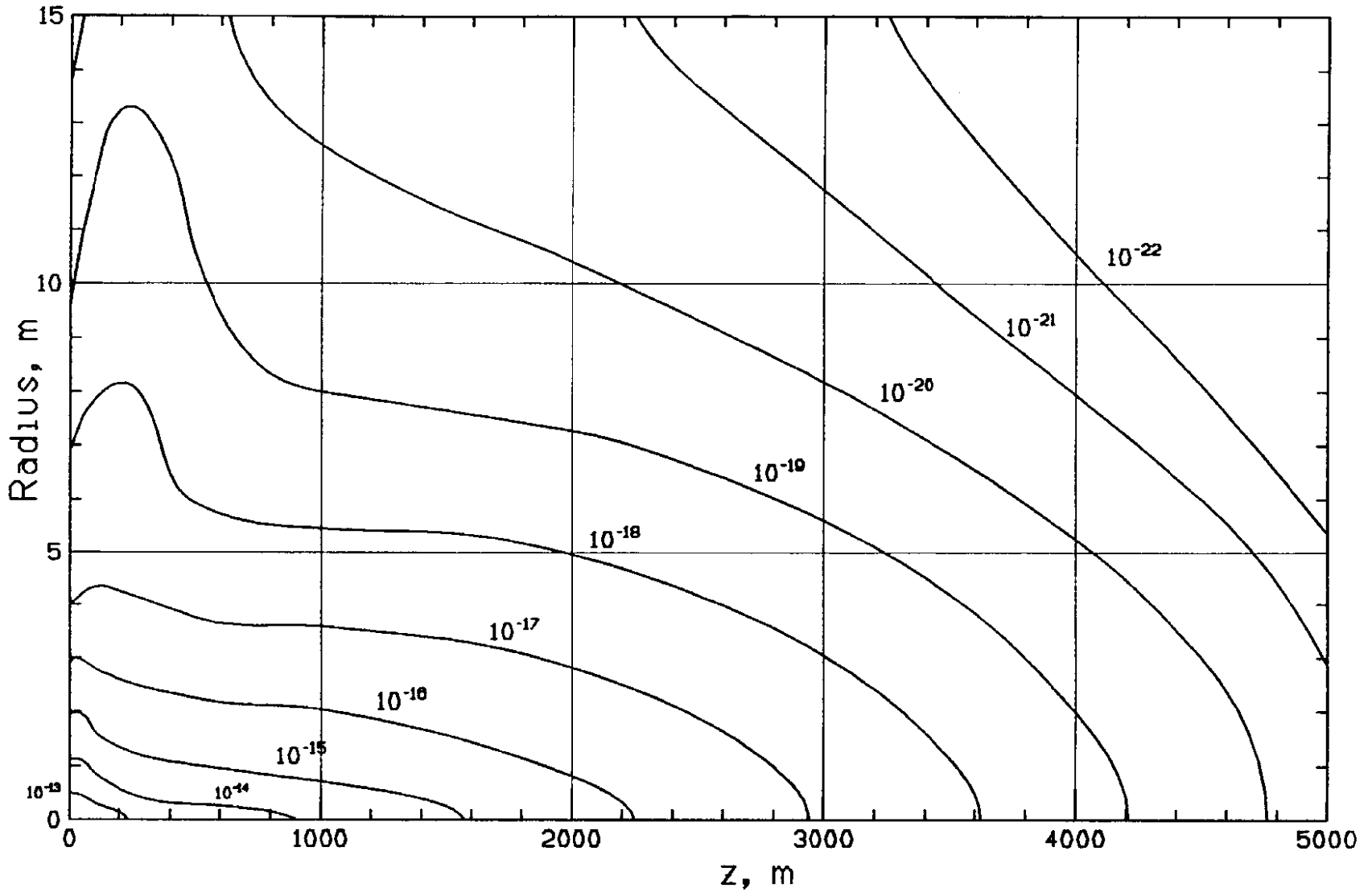

Fig. 5 Isodose contours due to muons in units of *rad/inc.proton* for 20 TeV protons incident on homogeneous soil as calculated by MUSIM program.

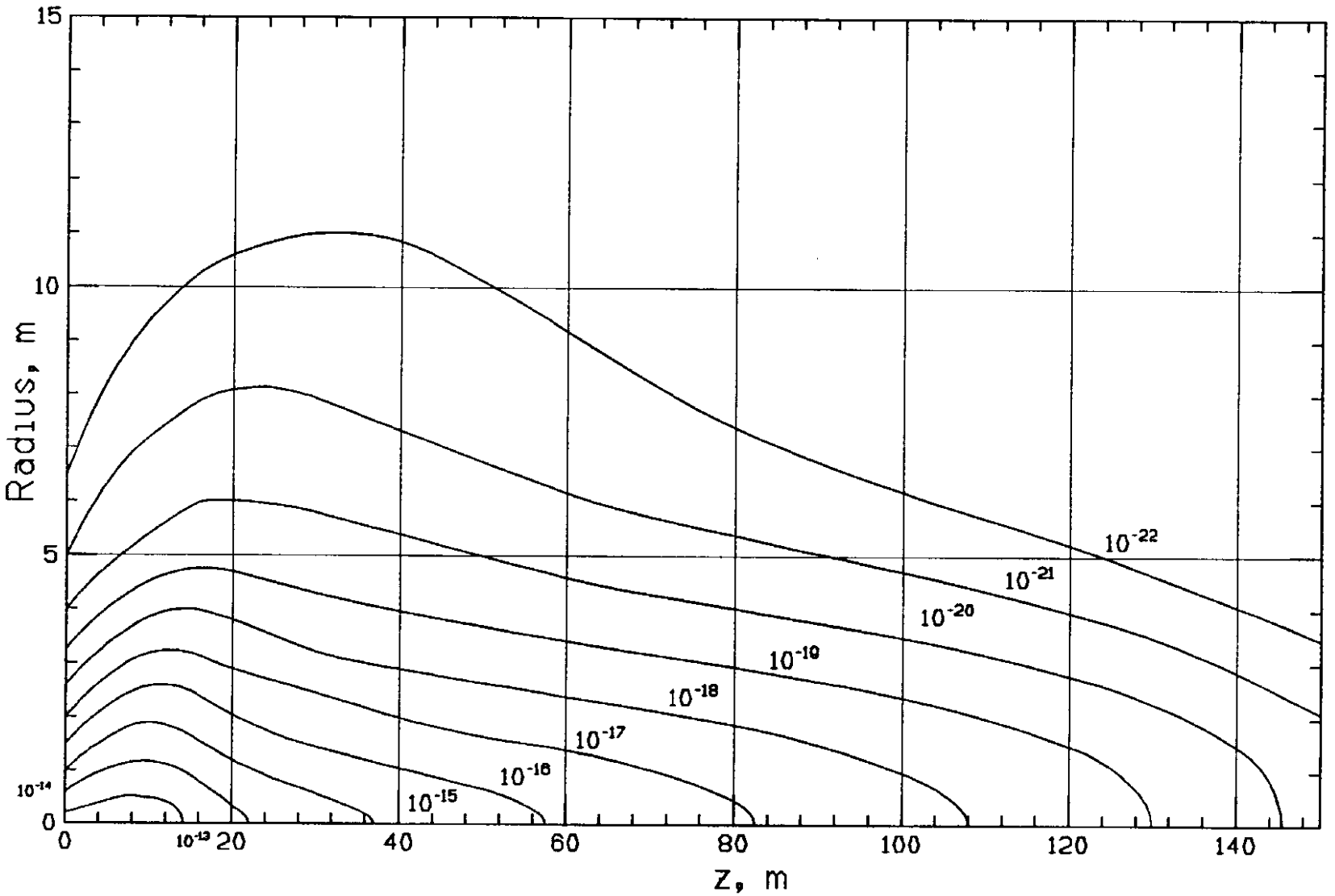

Fig. 6 Isodose contours due to muons in units of *rad/inc.proton* for 0.1 TeV protons incident on homogeneous soil as calculated by CASIMU program.

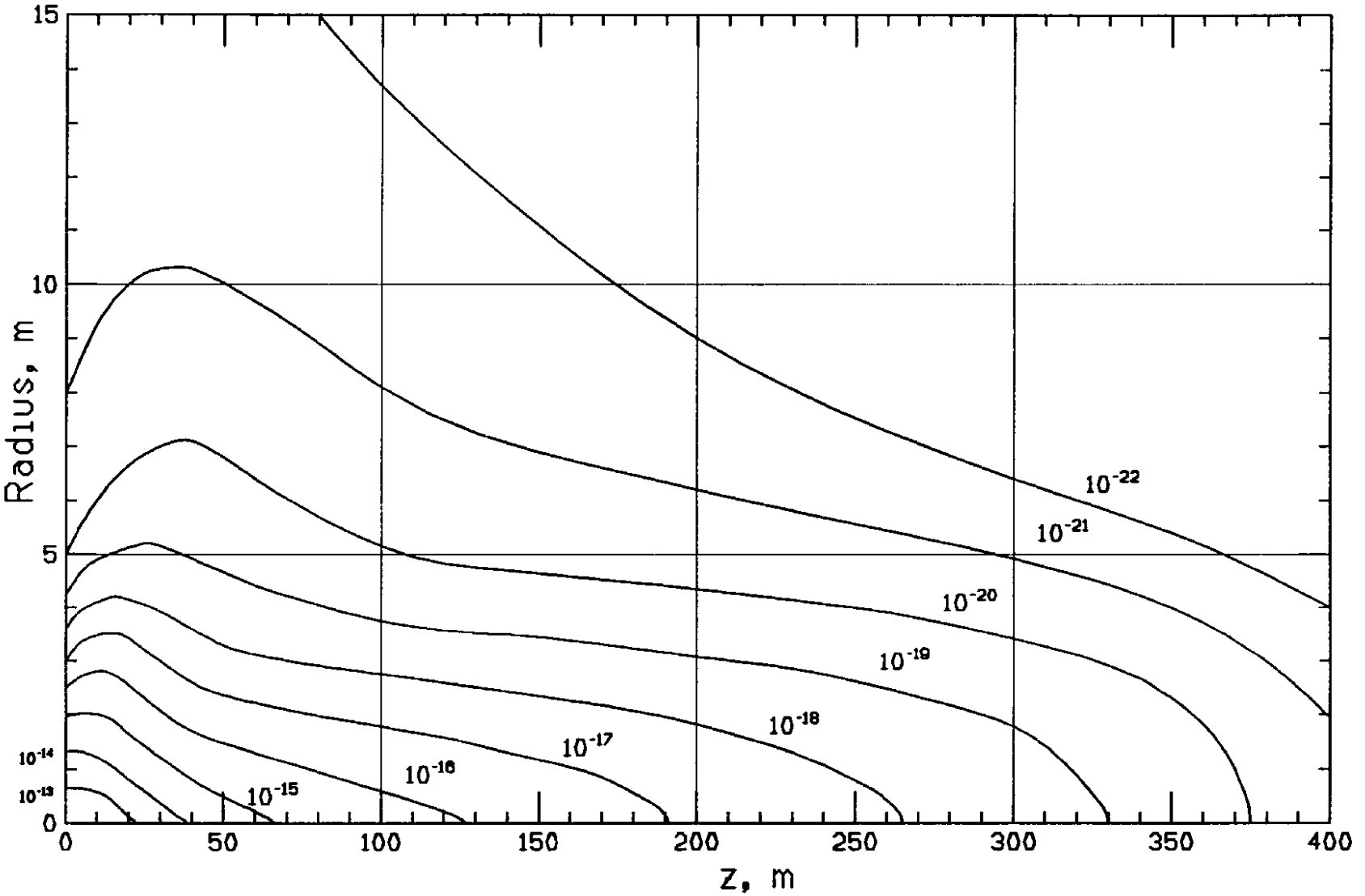

Fig. 7 Isodose contours due to muons in units of *rad/inc.proton* for 0.3 TeV protons incident on homogeneous soil as calculated by CASIMU program.

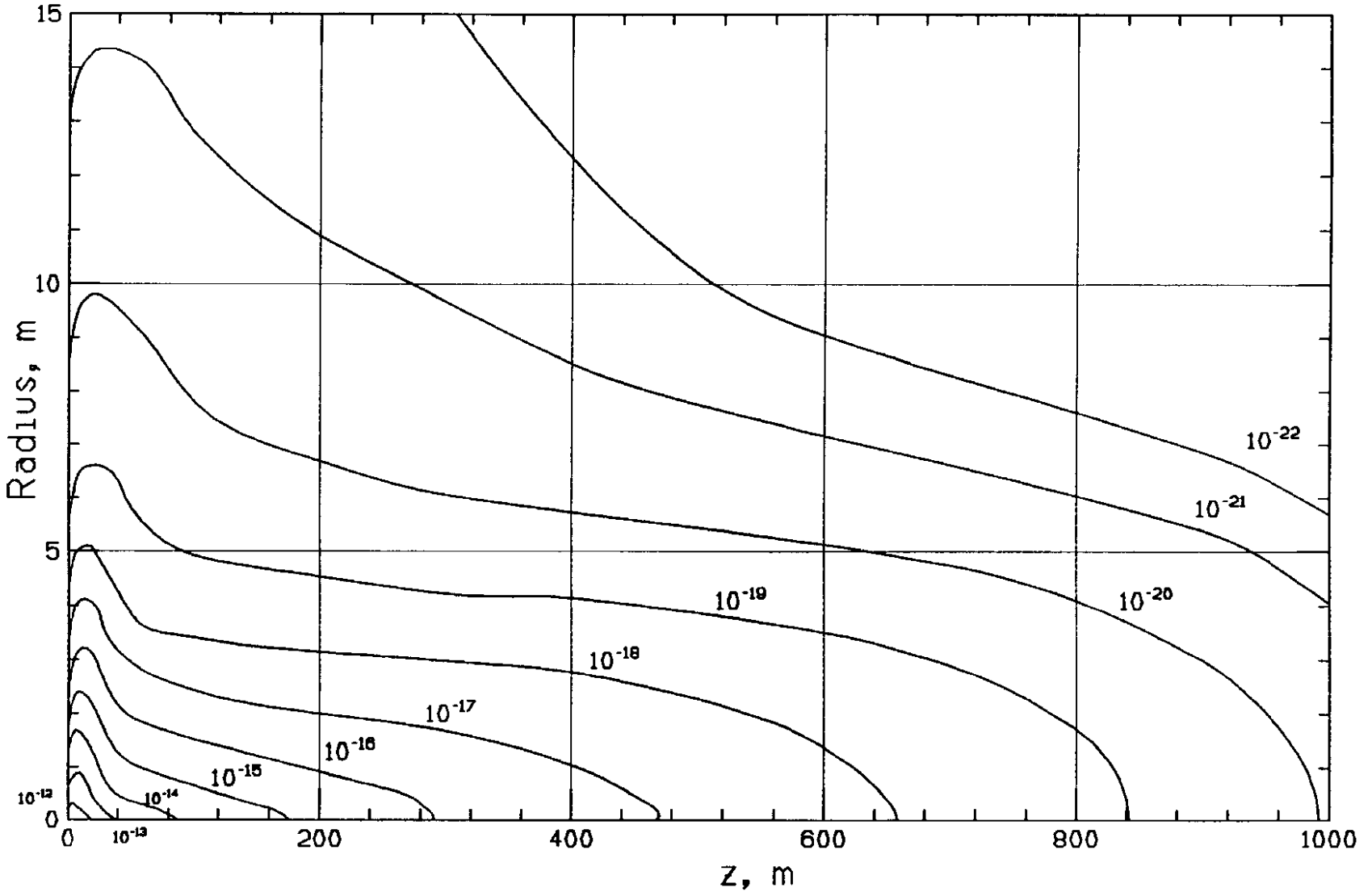

Fig. 8 Isodose contours due to muons in units of *rad/inc.proton* for 1 TeV protons incident on homogeneous soil as calculated by CASIMU program.

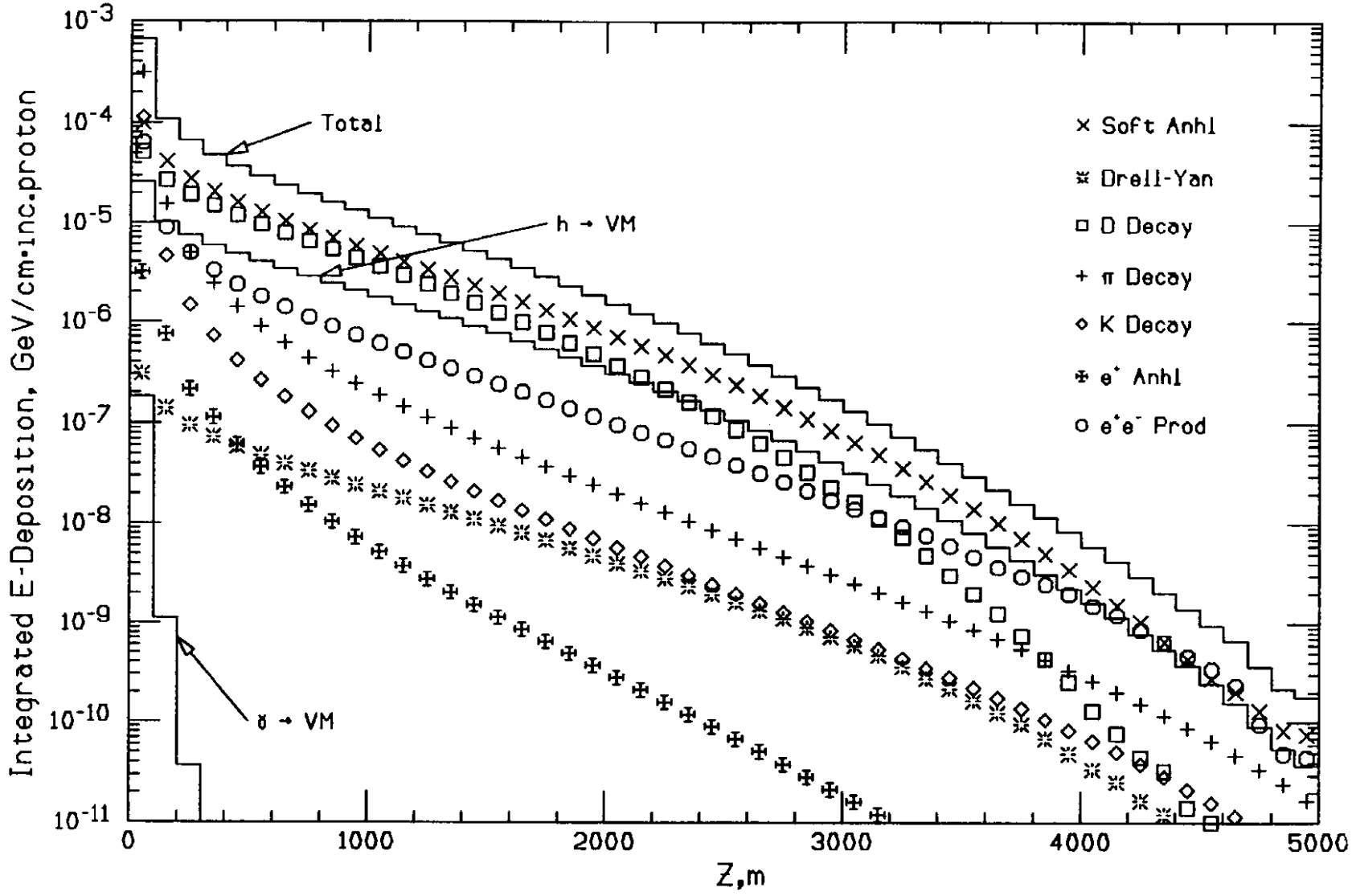

Fig. 9 Radially integrated muon energy deposition sorted by muon production mechanism as a function of longitudinal distance for 20 TeV protons incident on homogeneous soil as calculated by MUSIM program.

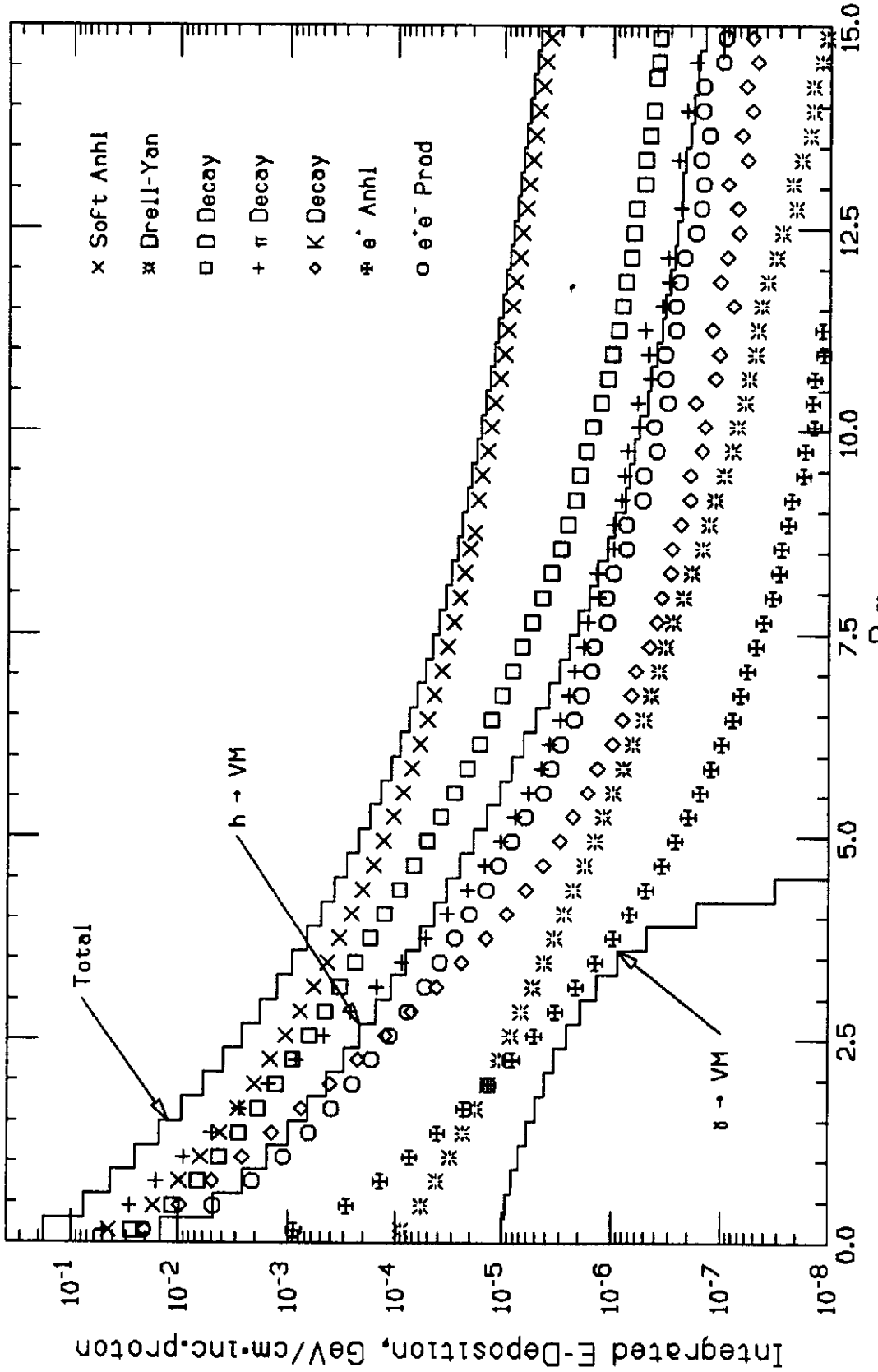

Fig. 10 Longitudinally integrated muon energy deposition sorted by muon production mechanism as a function of radius for 20 TeV protons incident on homogeneous soil as calculated by MUSIM program.

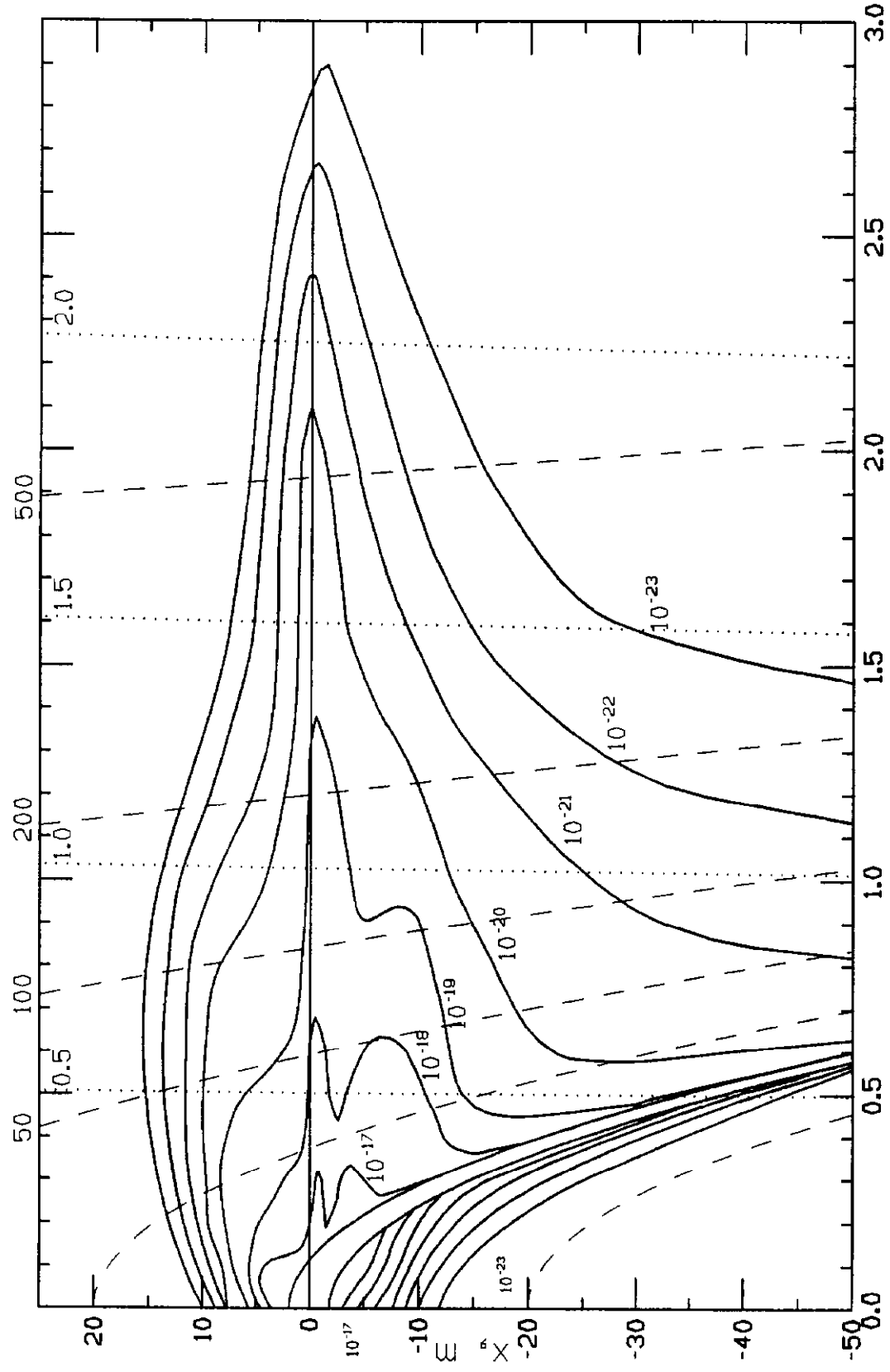

Fig. 11 Isodose contours due to muons in units of *Sv/inc.proton* for 8 TeV protons incident on the out-side of the vacuum chamber of a continuous dipole placed in the LEP tunnel.